Electric Modulus, Dielectric Relaxation Mechanism and Impedance Properties of Melaminum Perchlorate Monohydrate — Broadband Dielectric Spectroscopic Study

S. Sankar[a], N. Kanagathara[b] and J.C. Robinson Azariah[c]

[a] *Department of Physics, Indira Institute of Engineering & Technology, V.G.R. Nagar, Pandur, Thiruvallur District, 631 203, India*
[b] *Department of Physics, Saveetha School of Engineering, Saveetha Institute of Medical and Technical Sciences, Thandalam, Chennai 602 105, India*
[c] *Department of Electronics and Communication Engineering, Saveetha School of Engineering, Saveetha Institute of Medical and Technical Sciences, Thandalam, Chennai, 602 105, India*

Received: 01.12.2021 & Accepted: 02.02.2022

Doi: 10.12693/APhysPolA.141.500 *e-mail: kanagatharan.sse@saveetha.com

Single crystals of melaminium perchlorate monohydrate has been subjected to dielectric examination. Evaluation of electrical and dielectric mechanism of melaminium perchlorate monohydrate single crystals has been carried out over the temperature ranges from 313 to 373 K and frequency ranges from 0.05 to 5 MHz through dielectric, impedance spectral analysis and conductivity studies. At high frequencies, the dielectric constant and dielectric loss are found to be low for various temperatures, which ensures a good optical nature of the grown material. Complex impedance spectral analysis is involved in the study of the conduction and dielectric relaxation mechanism of the grown material. The frequency-dependent AC conductivity validates the Jonscher's power law. The formation of an asymmetric dispersion peak from the electrical modulus imaginary part (M'') indicates the non-Debye relaxation behaviour of the grown material. Thus in the present study, broadband dielectric spectroscopic investigation has been employed to analyse the mechanism of dielectric relaxation on melaminium perchlorate monohydrate.

topics: dielectric constant, conductivity, impedance, dielectric relaxation

1. Introduction

Materials with the desired properties and their certain application are based on characteristic including electrical, dielectric, magnetic, optical, and mechanical strength and toughness. In fact, all of the above properties are due to the internal structure of the material. Dielectric study plays a crucial role in wireless communication technology. According to the Maxwell–Wagner effect, the charge accumulation between two materials at the interface based on their difference in the charge carrier relaxation time. The dielectric constant (ε) and conductivity (σ) are the two factors needed to explain the electrical properties, and their ratio (ε/σ) gives the spreading and relaxation time of excess free carriers in materials [1].

Triazine derivatives has versatile applications in pharmacy, agriculture as a pesticide, potentiometric sensors for the determination of toxic metals, as a redox system in electrochemistry [2]. The dielectric properties of several s-triazine molecules were reported by Amal et al. [2]. The authors proved that the dielectric absorption of their s-triazine compounds made it possible to calculate the dielectric relaxation time. They have also reported that the high value of the dielectric constant indicates the semiconducting nature for all the samples [2].

Organic nonlinear optical (NLO) materials has a large demand in optical storage devices, colour display units and optical communication system etc. with optimum optical band gap and less dielectric constant. Triazine derivatives and its polymer have wide applications in variety of technological fields, including industry and engineering. Melamine is one such organic triazine molecule that is capable for nonlinear frequency conversion and its utilization. Much theoretical and experimental work has been done to analyse the nature of melamine in the solid form. Also, there have been many reports available on the dielectric properties of a few organic and inorganic materials melamine [3–10].

Recently we have reported the dielectric relaxation mechanism in melaminium bis (trichloroacetate) dihydrate [11]. As a continuation of the series with melamine, in this study, melaminium perchlorate monohydrate has been considered for dielectric spectroscopy, because there are no such reports available so far. Zhao and Shi reported the crystal structure of melaminium perchlorate monohydrate (MPM) [12]. Kanagathara et al. [13, 14] studied the X-ray diffraction, vibrational, thermal and dielectric nature of melaminium perchlorate monohydrate. It was revealed that the material is a triclinic system with a centrosymmetric space group ($P-1$) with lattice parameters: $a = 5.627$ Å, $b = 7.692$ Å, $c = 12.087$ Å, $\alpha = 103.89°$, $\beta = 94.61°$, $\gamma = 110.22°$ and volume = 468.95 Å^3 [14].

The intent of our attempt is to broaden our expertise about the electrical and dielectric mechanism of MPM and to determine the influence of grain interfaces on these properties. A detailed analysis of AC conductivity, electric modulus, dielectric modulus of MPM which yielded the highest conductivity is reported in this communication.

2. Material methods and characterization

MPM crystals were obtained by slow evaporation method with the precursor material as melamine and perchloric acid taken in an equimolar ratio (1:1) as described in [13]. A suitably polished MTCA crystal is subjected to dielectric characterization. DC voltage and capacitance is measured by LCR HITESTER HIOKI model 3532-50. The silver material slides are electroded with the aid of an air-drying silver paste. For the dielectric measurement, the temperature ranges from 313 to 373 K and frequency ranges from 0.05 to 5 MHz are used.

3. Results and discussion

3.1. Dielectric analysis

It turns out that electro–optical devices based on the modulation of the operating bandwidth with a very high operating frequency can be attained through a low dielectric constant at high frequencies in an organic material. Electrical properties are obtained as a function of temperature and frequency and can be studied with the help of dielectric analysis, which in turn allows access to the material's ability to store and transfer electrical charges. Figures 1 and 2 depict the dielectric constant and dielectric loss, respectively, as a function of logarithmic frequency $\log(F)$. It is seen in Fig. 1 that the dielectric constant decreases exponentially and reaches lower values at high frequencies. It is evident that all types of polarization (electronic, ionic, orientation and space charge) at low frequencies are effective and the dipoles easily align with the applied field. However, at higher frequencies, the dipoles themselves align difficult with the applied

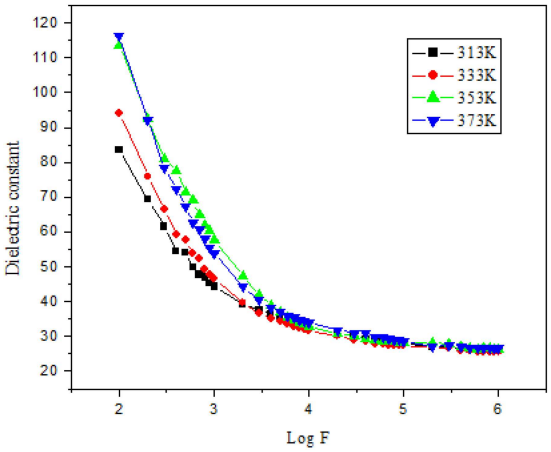

Fig. 1. Variation of dielectric constant vs $\log(F)$.

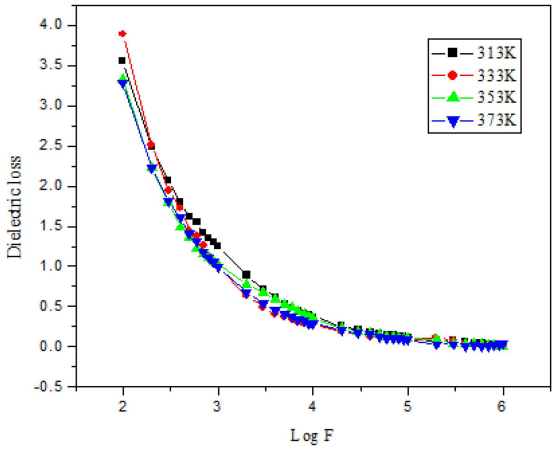

Fig. 2. Variation of dielectric loss vs $\log(F)$.

electric field and attains saturation. Hence, only electronic and ionic polarization exhibit at higher frequencies. The high value of the dielectric constant and the dielectric loss at low frequencies is an inherent property of the NLO material to be free from defect.

3.2. Broadband dielectric spectroscopic analysis

Broadband dielectric spectroscopic analysis includes dielectric dispersion, where the absorption phenomenon caused by the dipole relaxation arises from the reorientation movement of the dipoles, while electrical conductivity arises from the translational motion of electric charges (ions, electrons) in the vast frequency range. Intensive and extensive complex quantities are used in broadband dielectric spectroscopy to gain access to the dielectric and electric characteristics of the material [15]. Dipole relaxation is characterized in terms of dielectric permittivity ($\varepsilon*$) and conduction in terms of conductivity (σ), impedance (Z), electric modulus (M) and resistivity (ρ). The structure and molecular dynamics of materials are studied by broadband dielectric spectroscopy to quickly and

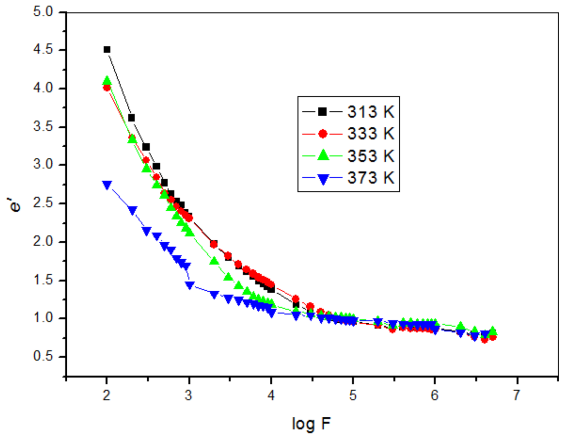

Fig. 3. Real dielectric constant vs log(F).

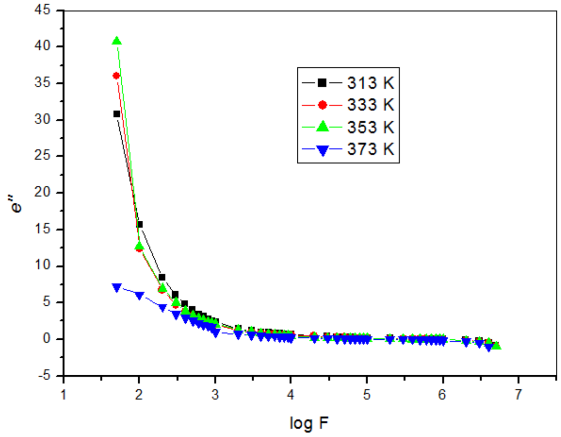

Fig. 4. Imaginary dielectric constant vs log(F).

efficiently obtain dielectric data in the frequency range 10^{-6}–10^{12} Hz. Besides, the changes in the dielectric constant and dielectric loss as a function of frequency, the impedance, the modulus and the conduction parameters are reported in detail in this communication.

3.2.1. Frequency vs real and imaginary dielectric constant

The frequency dependence of the dielectric constant and the dielectric loss at 313, 333, 353 and 373 K is shown in Figs. 3 and 4 and explains well how these parameters are associated with the polarization mechanism due to the electric filed [17, 18]. It is well known that, due to variation on the applied electrical field, the real and imaginary part represent the ability of materials to store and loss electrical energy, respectively. It is observed that both the real and the imaginary dielectric constant decrease with increasing frequency. However, at 313 K, the real dielectric constant is found to be high, and at 373 K, the imaginary dielectric constant is low. This infers that the dielectric polarization occurs as electronic, ionic (deformed) polatization in the high-frequency region, and relaxation polarization which includes orientation and interphase, occurs in the lower-frequency region [19]. Therefore the additional increase in frequency prevents the dipole from rotating freely and lags behind the electric field and attains a constant value [20, 21]. Thus all types of polarization play a role in which the electronic polarization is predominant over the other. Similar behaviour is observed in MTCA [11].

3.2.2. Complex impedance spectroscopic analysis

Complex impedance analysis is used to study the microstructure of materials and also overcome the drawback of interpreting the dielectric constant and dielectric loss depending on frequency. In general, the Cole–Cole plot is used for this impedance analysis by which the variation of dielectric parameters like permittivity, impedance, loss and electric modulus as a function of frequency is determined. This study also explain charge transport as well as relaxation mechanism in the material. The impedance data obtained is drawn in the complex plane. The high-frequency responses are due to the grains, and the low-frequency responses are due to the grain boundaries [22]. The real and imaginary complex impedance spectra of the grown material recorded at various temperatures is shown in Figs. 5 and 6, respectively.

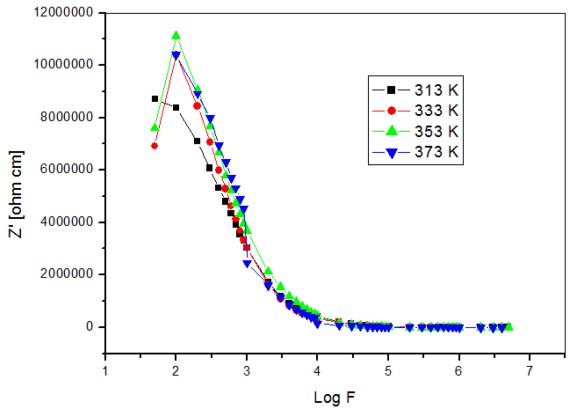

Fig. 5. Real impedance vs log(F).

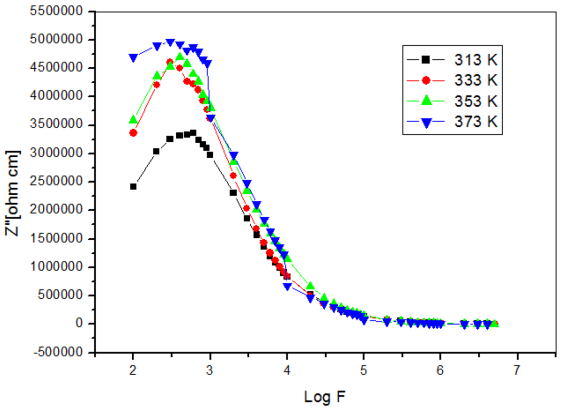

Fig. 6. Imaginary impedance vs log(F).

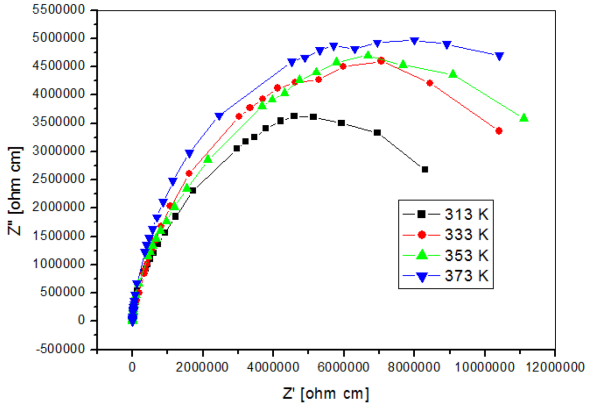

Fig. 7. Real vs imaginary impedance.

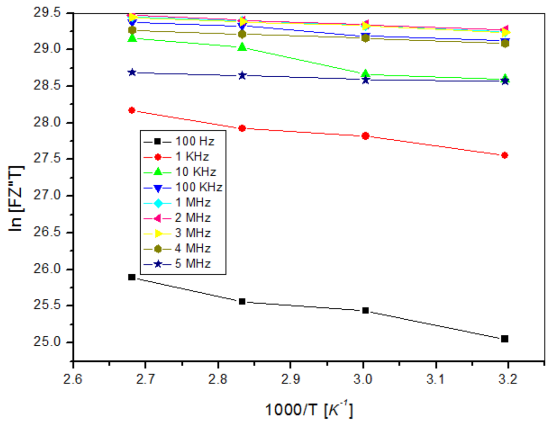

Fig. 8. Activation energy (E_a) obtained from impedance.

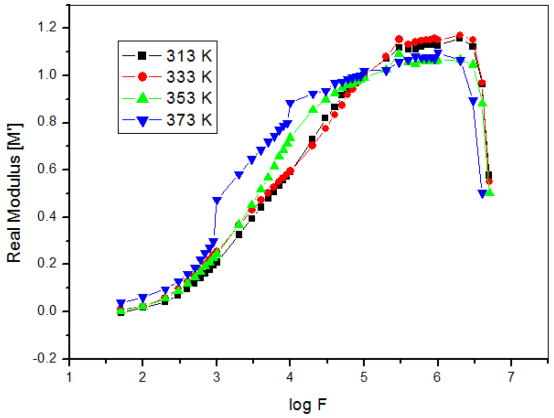

Fig. 9. Real modulus vs log(F).

TABLE I

Activation energy (E_a) obtained from impedance values.

Frequency F	E_a [eV]	Pre-exp. factor	R^2 value	Std. dev.
100 Hz	22.103	30.0064	0.9414	0.07325
1 kHz	21.656	31.1785	0.9559	0.0463
10 kHz	22.585	32.3149	0.9233	0.0921
100 kHz	10.114	30.7992	0.9678	0.0261
1 MHz	7.696	30.5309	0.9986	0.0069
2 MHz	7.438	30.5078	0.9966	0.0061
3 MHz	7.463	30.4884	0.9939	0.0082
4 MHz	6.754	30.2123	0.9994	0.0023
5 MHz	4.587	29.3268	0.9435	0.0159

Figure 7 represent the complex spectrum, and for temperatures ranging from 313 to 373 K, well-defined semicircles were obtained, and each experimental point corresponds to a frequency value. The semicircle diameter gives the resistivity and the maximum value corresponds to the relaxation frequency $\omega = \frac{1}{RC}$ [23]. When temperature increases, the arc radius corresponds to the decrease of the bulk resistance of the sample, indicating an activated mechanism of thermal conductivity. The centres of depressed semicircles on the line below the real axis indicate a deviation from the perfect Debye behaviour [24, 25]. There is a single semi-circle identified from the complex impedance spectrum for all temperatures. Also the grain boundary effect is marked with a semi-circle, and an increase in the grain size causes a decrease in the impedance value [26, 27].

Figure 7 shows the real and imaginary impedance as a function of frequency for four different temperatures 313, 333, 353 and 373 K. In both real and imaginary impedance, there is a small hump at low frequencies which then decreases and attains the saturation at larger frequencies. The activation energy estimated from the imaginary impedance for different frequencies is calculated (see Fig. 8) and given in Table I. It is seen that activation energy is high at lower frequencies, equal to around 22 eV.

3.2.3. Dielectric modulus studies

The combined knowledge of complex impedance and modulus studies that differentiates conduction mechanism and grain boundary effect are helpful to understand the dielectric characteristics [24]. The temperature–frequency-dependent real and imaginary electric modulus is shown in Fig. 9 and 10, respectively. Figure 9 shows changes in M' with frequency at the temperatures mentioned earlier. The curves indicate a very low value of M' in the low frequency region. The sigmoidal increase in M' with a frequency tending to M_∞ may contribute to the conduction mechanism due to short-range charge carriers mobility. Also, the M' value decreases with increasing temperature with well-dispersed curves where the region of dispersion shifts towards the region of higher frequency while simultaneously increasing the temperature. This dispersive nature validates long-range movement of charge carriers and implies a well-defined relaxation mechanism for all temperatures across the frequency [28]. Figure 10 shows the M'' variation as a function of frequency. It is observed that the increase in temperature

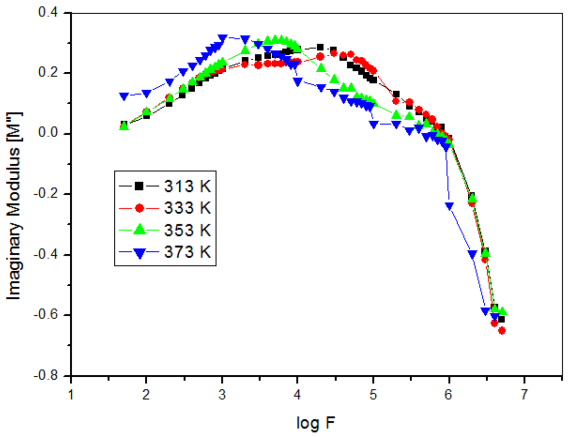

Fig. 10. Imaginary modulus vs $\log(F)$.

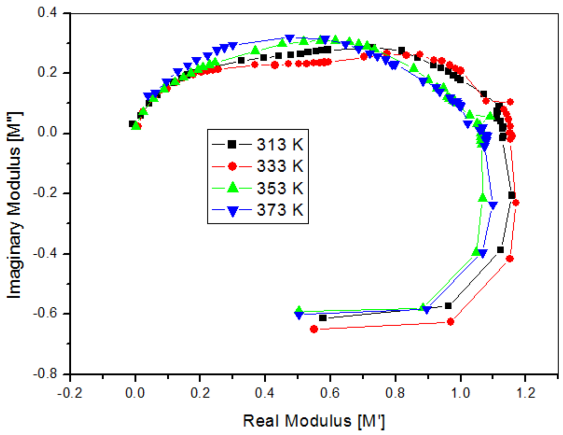

Fig. 11. Real vs imaginary modulus.

causes the maxima of the imaginary component of modulus ($M''_{\max}$) to shift towards the region of higher relaxation frequency. This behaviour suggests that thermally activated dielectric relaxation takes place, in which the hopping mechanism of charge carriers prevails [29]. The asymmetric peak broadening depicts the relaxation spread with various time constants, and the relaxation confirm the non-Debye nature of the material.

Figure 11 depicts the real as well as imaginary modulus of the material that indicates the presence of electrical relaxation in the material. There are two depressed semicircles that appear for all temperatures taken, however, at 373 K it seems to be high which is due to the grain boundary effect at lower frequencies. On the other hand, at high frequencies, this grain boundary effect has no distinct appearance in the Nyquist plot or the impedance plot. The bode plot (Fig. 12) was drawn by taking the logarithmic frequency along x-axis and the phase angle (θ) along y-axis. It is noticed from the Bode's plot that the peak is occurred at high frequencies for all temperatures, which indicates that the electrochemical reaction is faster since usually f represents the time constant of electrochemical

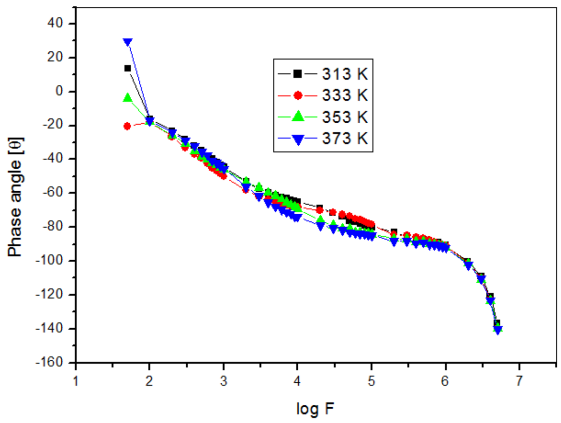

Fig. 12. Bode plot at different temperatures.

reaction [30]. Also the single peak in the frequency range implies the grain effect. By adjusting the grain size it is possible to tune the dielectric characteristics of the material.

3.2.4. Electrical conductivity studies

Frequency dependence of electrical conductivity obtained at various temperatures, i.e., 313, 333, 353 and 373 K, is plotted in Fig. 13. The results can be explained in three stages: low-frequency dispersion, plateau region and high-frequency region. The low-frequency dispersion is the first region which is due to the contribution of the polarization effect at the electrode and electrolyte interface. The second region is the frequency-independent conduction or DC conduction mechanism. It is noted that at low frequency there is less conductivity which is due to the accumulation of charges at the interface of electrode–electrolyte. However, at high frequencies there is no charge accumulation and the conductivity starts to increase rapidly, as proposed by Jonscher's power law [2, 31, 32]

$$\sigma_{\mathrm{AC}} = \sigma_o + \sigma_\omega. \tag{1}$$

Here σ_o is the frequency independent conductivity, σ_ω is the frequency dependent conductivity, given as

$$\sigma(\omega) = A\,\omega^s, \quad \text{with} \quad 0 \le s \le 1, \tag{2}$$

where ω — angular frequency of the applied AC field, and $A = \pi N^2 e^2/(12 k_{\mathrm{B}} T\,\alpha)$. Here, e is the electronic charge, T is the temperature, K_{B} is the Boltzmann constant, α is the polarizability of a pair of sites, and N is the number of sites per unit volume among which hopping takes place.

From the expression

$$\sigma = \frac{A}{2\pi\, fCd}, \tag{3}$$

where C is the capacitance, d is the thickness, A is the area of the crystal and f is the frequency of the applied field, one can calculate AC conductivity. Frequency dependent conductivity part is shown in Fig. 13. Frequency-independent conductivity is expressed as the plateau region at low

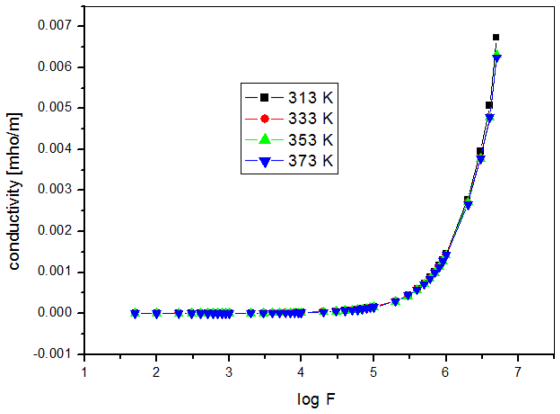

Fig. 13. Frequency dependence of electrical conductivity.

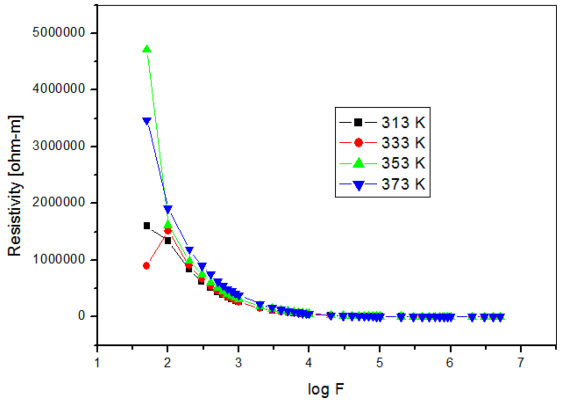

Fig. 14. Frequency dependence of electrical resistivity.

frequencies and the hopping frequency at higher frequencies. It is observed that an increase in frequency results in an increase in conductivity by obeying the Jonscher's power [33–35]. Also, it is noted that the conduction process is very low up to 100 kHz, and beyond 100 kHz the conductivity starts to increase and establishes that the material MPM undergoes a thermally activated process. Figure 14 represents the frequency-dependent resistivity behaviour where the decrease in resistivity occurs with increasing frequency.

4. Conclusion

Broadband dielectric spectroscopic investigation has been employed to analyse the mechanism of dielectric relaxationon melaminium perchlorate monohydrate (MPM) single crystal. MPM crystal exhibit the maximum of dielectric constant and loss at low frequencies which is the inherent property of the NLO material to be free from defect.

The electric modulus and complex impedance spectra were recorded. From the complex impedance spectrum, a single semi-circle is identified for all temperatures. The semi-circle represents a grain boundary effect, and an increase in grain size decreases the impedance value. The effective activation energy calculated from the impedance values is found to be higher at lower frequencies, representing thermally activated conduction mechanism. The presence of single semi-circle in the temperature–frequency dependent real and imaginary electric modulus indicates the existence of grain boundary effect in the material. The formation of asymmetric dispersion peak from the imaginary part (M'') of the electrical modulus indicates the non-Debye relaxation behaviour of the material. The Jonscher's power law is applied to describe the mechanism of conductivity, which clearly states that AC conductivity starts to increase with increase in hopping frequency. Thus AC conductivity variation with frequency obeys Jonscher's law. Thus the normal dielectric behaviour of the MPM material is established in this communication.

References

[1] M. Iwamoto, *Encyclopedia of Nanotechnology*, Springer Science + Business Media Dordrecht., 2015.

[2] M. Amal, A. Karim, A.H. Salama, A. Fatma, E. Samahy, M. El-Sedik, F.H. Osman, *J. Phys. Org. Chem.* **30**, 3703 (2017).

[3] V. Sangeetha, M. Govindarajan, N. Kanagathara, M.K. Marchewka, S. Gunasekaran, G. Anbalagan, *Spectrochim. Acta A* **118**, 1025 (2014).

[4] N. Kanagathara, M.K. Marchewka, M. Drozd, P.R. Rajakumar, S. Gunasekaran, G. Anbalagan, *Spectrochim. Acta A* **145**, 394 (2015).

[5] N. Kanagathara, N.G. Renganathan, M.K. Marchewka, N. Sivakumar, K. Gayathri, P. Krishnan, S. Gunasekaran, G. Anbalagan, *Spectrochim. Acta A* **101**, 112 (2013).

[6] N. Kanagathara, M.K. Marchewka, N.G. Renganathan, S. Gunasekaran, G. Anbalagan, *J. Mol. Struc.* **1049**, 345 (2013).

[7] V. Sangeetha, M. Govindarajan, N. Kanagathara, M.K. Marchewka, M. Drozd, G. Anbalagan, *J. Mol. Struc.* **1054**, 307 (2013).

[8] V. Sangeetha, K. Gayathri, P. Krishnan, N. Sivakumar, N. Kanagathara, G. Anbalagan, *J. Therm Anal. Calorim.*, **117**, 307 (2014).

[9] V. Sangeetha, K. Gayathri, P. Krishnan, N. Sivakumar, N. Kanagathara, G. Anbalagan, *J. Cryst. Growth* **389**, 30 (2014).

[10] N. Sivakumar, N. Kanagathara, G. Bhagavannarayana, S. Kalainathan, G. Anbalagan, *J. Cryst. Growth* **426**, 86 (2015).

[11] S. Sankar, N. Kanagathara, V. Natarajan, C.R.A. John Chelliah, *J. Mater. Sci. Mater. Electron* **32**, 10778 (2021).

[12] M.M. Zhao, P.P. Shi, *Acta Cryst. E* **66**, o1463 (2010).

[13] N. Kanagathara, M.K. Marchewka, N. Sivakumar, K. Gayathri, N.G. Renganathan, S. Gunasekaran, G. Anbalagan, *J. Therm. Anal. Calorim.* **112**, 1317 (2013).

[14] N. Kanagathara, M.K. Marchewka, M. Drozd, N.G. Renganathan, S. Gunasekaran, G. Anbalagan, *Spectrochim. Acta A* **112**, 343 (2013).

[15] S.K. Rout, A. Hussian, J.S. Lee, I.W. Kim, S.I. Woo, *J. Alloys Compd.* **477**, 706 (2009).

[16] Siva Vadivel, A. Shameem, A. Murugan, *J. Mol. Struc.* **1205**, 127619 (2019).

[17] R. Mesbeh, B. Hamdi, R. Zouari, *Ionics* **25**, 6147 (2019).

[18] P. Venkaterwarlu, A. Laha, S.B. Krupanidhi, *Thin Solid Films* **474**, 1 (2005).

[19] B. Tareev, A. Ttroitsky, *Physics of dielectric materials*, Mir Publishers Moscow, 1975.

[20] S. Kurien, J. Mathew, S. Sebastian, S.N. Potty, K.C. George, *Mater. Chem. Phys.* **98**, 470 (2006).

[21] P.S. Anantha, K. Harihanan, *Mater. Sci. Eng. B* **121**, 12 (2005).

[22] P. Victor, S. Bhattacharyya, S.B. Krupanidh, *J. Appl. Phys.* **94**, 5135 (2003).

[23] Z.S. Macedo, C.S.S. Oliveira, *J. App. Phys.* **102**, 034105 (2007).

[24] D.C. Sinclair, A.R. West, *J. Appl. Phys.* **66**, 3850 (1989).

[25] A. Ben Rhaiem, K. Guidara, M. Gargouri, A. Daoud, *J. Alloys Compd.* **392**, 68 (2005).

[26] R. Tripathi, A. Kumar, T.P. Sinha, *Pramana* **72**, 969 (2009).

[27] Haibado Mahamoud, Bassem Louati, Faouzi Hlel, Kamel Guidara, *Ionics* **17**, 223 (2011).

[28] P.S. Das, P.K. Chakraborty, B. Behera, R.N.P. Choudhary, *Phys. B* **395**, 98 (2007).

[29] B.Behera, P.Nayak, R.N.P.Choudhary, *Mater. Res. Bull* **43**, 401 (2008).

[30] Duduzile Nkosi, Jeseelan Pillay, Kenneth I. Ozoemena, Khalid Nounehc, Munetaka Oyama, *Phys. Chem. Chem. Phys.* **12(3),** 604 (2010).

[31] S. Ayesha, S. Austin Suthanthiraraj, *Chem. Sci. Trans.* **3**, 847 (2014).

[32] C.R.A. John Chelliah, R. Swaminathan, *J. Mater. Sci. Mater. Electron* **31**, 7348 (2020).

[33] A.K. Jonscher, *Nature* **267**, 673 (1977).

[34] Yan Li, Yonghao Han, Yanzhang Ma, Pinwen Zhu, Xin Wang, Chunxiao Gao, *EPL*, **98**, 1 (2012).

[35] N. Kanagathara, G. Anbalagan, *Inter. J. Optics* **826763**, 1 (2012).